J|A|C|S ARTICLES

Published on Web 05/07/2010

Efficient Calculation of Diffusion Limitations in Metal Organic Framework Materials: A Tool for Identifying Materials for Kinetic Separations

Emmanuel Haldoupis, Sankar Nair, and David S. Sholl*

School of Chemical & Biomolecular Engineering, Georgia Institute of Technology, 311 Ferst Drive, Atlanta, Georgia 30332-0100

Received March 25, 2010; E-mail: david.sholl@chbe.gatech.edu

Abstract: The very large number of distinct structures that are known for metal−organic frameworks (MOFs) and related materials presents both an opportunity and a challenge for identifying materials with useful properties for targeted applications. We show that efficient computational models can be used to evaluate large numbers of MOFs for kinetic separations of light gases based on finding materials with large differences between the diffusion coefficients of adsorbed gas species. We introduce a geometric approach that rapidly identifies the key features of a pore structure that control molecular diffusion and couple this with efficient molecular modeling calculations that predict the Henry's constant and diffusion activation energy for a range of spherical adsorbates. We demonstrate our approach for >500 MOFs and >160 silica zeolites. Our results indicate that many large pore MOFs will be of limited interest for separations based on kinetic effects, but we identify a significant number of materials that are predicted to have extraordinary properties for separation of gases such as CO_2, CH_4, and H_2.

1. Introduction

Metal organic frameworks (MOFs) are a class of microporous materials that consist of inorganic secondary building units (SBU) connected together with organic linkers to form a three-dimensional framework. These materials can be synthesized with a variety of pore environments by combining SBUs with organic linkers of different length, conformation, and functionalization. The exploitation of the properties of MOFs is being actively investigated using both experiments and simulations for a range of applications.[1] One of the challenges involved developing applications using MOFs is the huge number of distinct structures that are known.[2] Methods that can rapidly examine a large number of possible structures to reliably identify a small number of candidate materials suitable for a particular application are therefore of considerable value.

Chemical separations involving molecular adsorption into nanopores can be broadly classified as equilibrium separations or kinetic separations.[3] The selectivity of an equilibrium separation is controlled by the adsorption affinity of the adsorbent for one species relative to another. In a kinetic separation, in contrast, selectivity is accomplished due to different transport rates of chemical species through pores in the adsorbent. One use of kinetic separations is via cyclic operation of packed beds; this concept is practiced commercially for O_2/N_2 separations.[3] Kinetic separations are also crucial in applications of membranes, where the net selectivity of a membrane is governed by a combination of adsorption selectivity and selectivity due to molecular diffusion.[4] In the most extreme case, kinetic separations can occur by molecular sieving, where molecules of the larger (smaller) species cannot (can) diffuse through an adsorbent's pores. For molecules that are similar in size, such as O_2/N_2, CO_2/CH_4, or *o*-/*p*-xylene, it is typically not possible to perform the idealized molecular sieving just described. It is possible, however, to find pores that allow both species to diffuse with very different transport rates. Examples of materials of this kind include carbon molecular sieves for light gas separations[5] and zeolites such as DDR and SAPO-34 for CO_2/CH_4 separations.[6,7]

The properties of MOFs are in many ways ideally suited to the challenge of developing nanoporous materials for kinetic separations. Indeed, experimental and computational investigations have recently identified examples of MOFs with great potential for this goal.[8,9] Ideally, one would like to select a small number of MOFs from the large variety of materials that are known that have promise for a desired kinetic separation before performing extensive experimental studies of any specific material. A minimal requirement for this task is the ability to define the portions of the pores inside a material that will limit net diffusion of an adsorbed molecule. This task is more challenging than simply characterizing the available pore volume, since materials can

(1) Ferey, G. *Chem. Soc. Rev.* **2008**, *37*, 191.
(2) Long, J. R.; Yaghi, O. M. *Chem. Soc. Rev.* **2009**, *38*, 1213.
(3) Yang, R. T. *Gas Separation by Adsorption Processes*; Butterworths: Boston, 1987.
(4) Baker, R. W. *Membrane Technology and Applications*; McGraw-Hill: New York, 2000.
(5) Jones, C. W.; Koros, W. J. *Carbon* **1994**, *32*, 1419.
(6) Carreon, M. A.; Li, S.; Falconer, J. L.; Noble, R. D. *J. Am. Chem. Soc.* **2008**, *130*, 5412.
(7) Jee, S. E.; Sholl, D. S. *J. Am. Chem. Soc.* **2009**, *131*, 7896.
(8) Pan, L.; Olson, D. H.; Ciemnolonski, L. R.; Heddy, R.; Li, J. *Angew. Chem., Int. Ed.* **2006**, *45*, 616.
(9) Watanabe, T.; Keskin, S.; Nair, S.; Sholl, D. S. *Phys. Chem. Chem. Phys.* **2009**, *11*, 11389.

10.1021/ja1023699

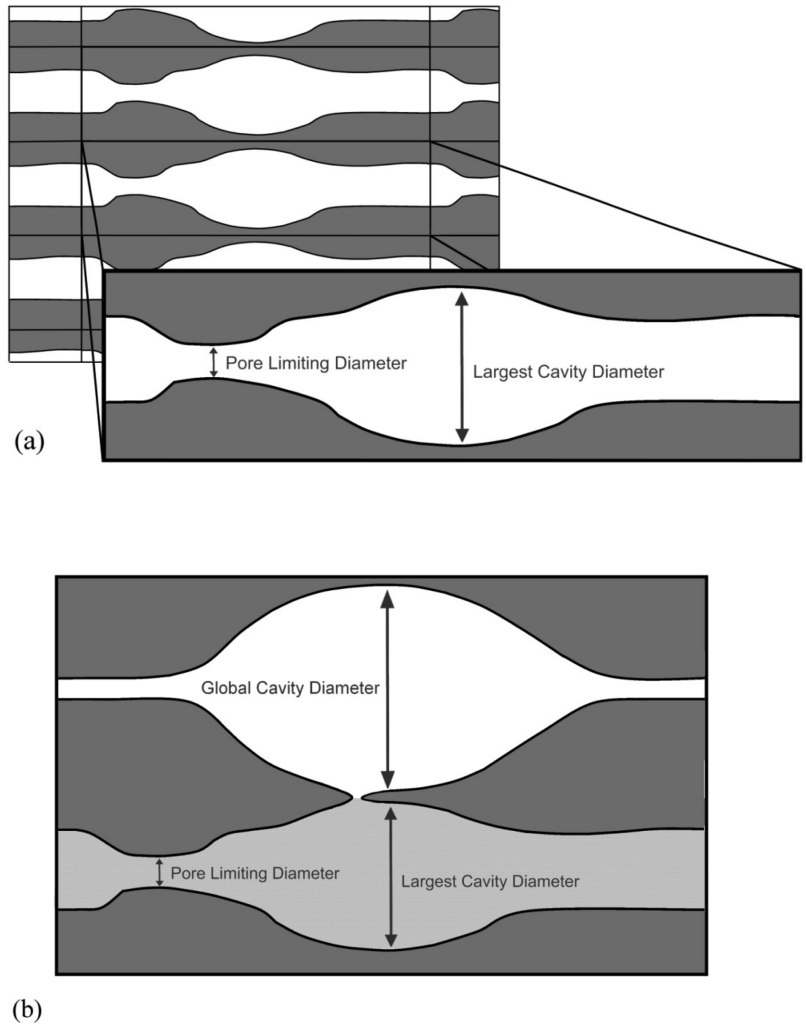

Figure 1. (a) Two-dimensional schematic representation of a periodic nanoporous channel system. The pore-limiting diameter and the largest cavity diameter have been highlighted in one of the unit cells. (b) Schematic illustration of a single unit cell of a material where the global cavity diameter is outside the major pore, which has been colored light gray.

potentially have large open cavities that are connected by narrow pores. In materials of this type, it is the narrow pores that will determine how molecules diffuse. Although a purely geometric characterization of a material is very useful, it is not sufficient to estimate the potential of a given structure, since the unique chemical environment of the pores in each structure can greatly affect the selectivity and permeability. Therefore, it is also critical to develop efficient calculations that include a description of the molecular interactions between the diffusing molecules and the MOF framework.

In this paper, we demonstrate an efficient "hierarchical" method for characterizing the pores that control molecular diffusion through MOFs on the basis of information from experimental crystal structures. This method also provides a simple characterization of the cavity volumes that exist within a material. Beyond these geometric calculations, we demonstrate how the adsorption affinity (in the form of the Henry's constant) and the diffusion rate of molecules can be estimated efficiently for a large number of structures. Our methods for all these calculations are described in detail in section 2. In section 3.1, we validate our results by applying the method to more than 150 zeolite structures that have been characterized previously with a different method by Foster et al.[10] This comparison highlights several advantages of the methods we have developed. In sections 3.2−3.4, we present results of applying our procedure to more than 500 MOF structures. We discuss the significance of our results for a large group of MOFs and for CH_4 and H_2 as adsorbates. We also discuss our predictions in light of several recent reports on MOF membrane fabrication and characterization.

2. Theoretical Calculations

2.1. Pore Size Characterization. Pores in crystalline materials can have a large variety of shapes and connectivities. Since the goal of this work is to estimate the potential that a material has for kinetic separations, we aim to quantify the features of the pore inside a structure that control diffusion of adsorbed molecules. We do so by defining the pore-limiting diameter as illustrated in Figure 1a (in two dimensions). The pore-limiting diameter is defined such that it is impossible for any sphere with a diameter larger than the pore-limiting diameter of a structure to travel through this structure without overlapping one or more framework atoms. Although real molecules are not hard spheres, it is clear that gas molecules that

(10) Foster, M. D.; Rivin, I.; Treacy, M. M. J.; Delgado Friedrichs, O. *Microporous Mesoporous Mater.* **2006**, *90*, 32.

are significantly smaller (larger) than the pore-limiting diameter of a porous material will be able to diffuse freely (will have at most very slow diffusion) through the material. As a result, knowledge of this quantity can be used to make a decision concerning the potential of a structure for a specific kinetic separation. This quantity has been referred to previously as the maximum free sphere for a porous material.[10,11] Some porous materials can contain multiple networks of channels that have limited interconnectivity. In these cases, we label the connected set of pores that includes the constriction that generates the pore-limiting diameter as the major channel. A two-dimensional example of a material in which this concept is relevant is shown in Figure 1b. The major channel sets the limit on the size of molecules that can diffuse throughout the material. Another quantity of interest that can influence the way molecules diffuse is the largest cavity diameter, defined as the largest spherical particle that can be inserted at some point within the material's pores without overlapping with any framework atoms. This quantity is shown in two dimensions in Figure 1. By definition, the smallest possible value of the largest cavity diameter is the pore-limiting diameter. This would be true for a perfectly cylindrical channel; an example of this would be a carbon nanotube. For most cases, however, the largest cavity diameter is larger than the pore-limiting diameter, and it is clear that a probe molecule the same size as the largest cavity diameter cannot diffuse through the material. This quantity is also known as the maximum included sphere.[10,11]

The importance of the largest cavity diameter to kinetic separations can be understood by considering the possible outcomes when a slowly diffusing species and a smaller, more rapidly diffusing species are both present in a material's pores. If the smaller molecules are unable to readily pass the larger molecules within some portion of the pores, then the diffusion rate of the smaller molecules in the adsorbed mixture will be dominated by the slowly diffusing species. This is a very undesirable outcome if an effective kinetic separation is desired. Single-file diffusion in mixtures inside one-dimensional pores offers an extreme example of this phenomenon.[12−14] This qualitative description suggests that to be most useful for kinetic separations, a porous material should have a pore-limiting diameter of a size that is appropriate to create a strong transport-based separation but a largest cavity diameter large enough to allow facile mixing of molecules within the material's cavities.

We have developed efficient methods to calculate the pore-limiting diameter and largest cavity diameter based on the insertion of spherical particles into a crystalline porous structure in which the positions of framework atoms are fixed. There are, of course, many examples of MOFs in which framework flexibility plays an important role in molecular adsorption.[15−17] Because of the efficiency of the methods described below, it would be straightforward to examine the characteristics of a MOF's pore structure as its framework coordinates were varied to describe a flexible structure. It is important that these calculations can describe the full range of atomic species that are present in MOFs. To this end, we use the van der Waals (vdW) radii defined by the Cambridge Structural Database (CSD) to assign a size to each framework atom. These values were developed for most elements by Bondi[18] and for H by Rowland and Taylor.[19] Some elements were not treated by Bondi, and the CSD assigns an arbitrary value of 2 Å for these elements. To be more consistent, we used Pauling's approximation as reported in Bondi's paper, which assigns the vdW radius to be 0.75 Å larger than the element's covalent radius. The covalent radii were obtained from Cordero et al.[20]

Our calculation begins by dividing a crystallographic unit cell into discrete grid points equally spaced along the three crystallographic axes. At each grid point, the distances between the grid point and the complete set of framework atoms is calculated, allowing the maximum possible probe size for that grid point to be recorded. Periodic boundary conditions are used in this and all following calculations. The largest probe size that is observed for any grid point in this calculation defines the material's largest cavity diameter. This calculation is exact in the limit of very small grid spacings but introduces a well-defined level of uncertainty when applied using a finite grid spacing.

To establish the pore-limiting diameter, the connectivity of pores within the material must be determined. We do this using an efficient multiple-labeling algorithm introduced by Hoshen and Kopelman[21] in the context of analyzing percolation in simple lattices. This calculation begins by identifying all grid points at which probe particles of a given size could be located without overlapping framework atoms. It is assumed that if two neighboring grid points are both feasible locations for a probe particle then the probe particle can be moved continuously between the grid points without overlapping any framework atoms. If a set of feasible grid points exists that allows the probe particle to be moved in this way for an unlimited distance through the crystal, then this probe particle is smaller than (or equal to) the pore-limiting diameter. The Hoshen−Kopelman algorithm efficiently identifies and labels clusters of connected grid points. Clusters which connect points on opposite sides of the crystallographic unit cell are called, in the language of percolation theory, spanning clusters. When the cluster-labeling procedure is finished, the resulting clusters are checked to identify spanning clusters. This procedure correctly identifies any path that allows a diffusion path of infinite extent through the material; it is not limited to paths oriented along the principal crystallographic directions. The pore-limiting diameter corresponds to the largest probe sphere diameter that is found to result in at least one spanning cluster. Similar to the calculation of the largest cavity diameter, this calculation is exact in the limit of infinitesimal grid spacings and introduces a well-defined level of uncertainty when applied with a finite grid spacing.

Once we have characterized a pore structure as described above, visualization of the spanning cluster associated with the pore-limiting diameter offers a simple way to visualize the pores accessible to diffusing molecules. In some materials, the largest cavity diameter defined above does not fall within the major channel. Our calculations detect this situation automatically and allow the maximum cavity size within the accessible region to be calculated. As well as being useful for classifying materials, this capability will be useful for avoiding the inclusion of inaccessible volumes during simulation of adsorption with Grand Canonical Monte Carlo, an issue that has been highlighted recently by Krishna and van Baten.[22]

The algorithm we have described above is highly efficient; even large crystallographic unit cells that contain many hundreds of atoms can be analyzed in a few minutes using a single processor. Calculations for materials with smaller unit cells can be completed in seconds. The upper bound on the uncertainty in the calculated diameters can be estimated, for an orthogonal unit cell, to be $\sqrt{3}\cdot d$, where d is the grid spacing. Use of a grid spacing of 0.1 Å, as we do for the MOF calculations reported below, is therefore associated with an uncertainty of 0.17 Å. For materials found to be of particular interest, it is simple to reduce the size of this uncertainty by using a smaller grid spacing.

(11) Li, H.; Eddaoudi, M.; O'Keeffe, M.; Yaghi, O. M. *Nature* **1999**, *402*, 276.
(12) Sholl, D. S.; Fichthorn, K. A. *Phys. Rev. Lett.* **1997**, *79*, 3569.
(13) Sholl, D. S.; Fichthorn, K. A. *J. Chem. Phys.* **1997**, *107*, 4384.
(14) Kukla, V.; Kornatowski, J.; Demuth, D.; Girnus, I.; Pfeifer, H.; Rees, L. V. C.; Schunk, S.; Unger, K. K.; Kärger, J. *Science* **1996**, *272*, 702.
(15) Ferey, G.; Serre, C. *Chem. Soc. Rev.* **2009**, *38*, 1380.
(16) Ramsahye, N. A.; Maurin, G.; Bourrelly, S.; Llewellyn, P. L.; Loiseau, T.; Serre, C.; Ferey, G. *Chem. Commun.* **2007**, 3261.
(17) Seki, K. *Phys. Chem. Chem. Phys.* **2002**, *4*, 1968.
(18) Bondi, A. *J. Phys. Chem.* **1964**, *68*, 441.
(19) Rowland, R. S.; Taylor, R. *J. Phys. Chem.* **1996**, *100*, 7384.
(20) Cordero, B.; Gomez, V.; Platero-Prats, A. E.; Reves, M.; Echeverria, J.; Cremades, E.; Barragan, F.; Alvarez, S. *Dalton Trans.* **2008**, 2832.
(21) Hoshen, J.; Kopelman, R. *Phys. Rev. B* **1976**, *14*, 3438.
(22) Krishna, R.; van Baten, J. M. *Langmuir* **2010**, *26*, 2975.

2.2. Adsorption and Diffusion Calculations for Spherical Adsorbates. The methods presented above have examined MOFs from a purely geometric viewpoint. The information extracted from this geometric analysis, however, can also be used to efficiently characterize several useful properties of adsorbed molecules in MOFs. In this section, we pursue this concept by determining the Henry's constant for adsorption of spherical adsorbates and estimating the activation energy associated with net diffusion of the same adsorbates in a large number of MOFs. To illustrate our approach, we concentrate on the properties of CH_4 in MOFs, but we also show how our results can easily be extended to a range of other adsorbates.

To describe molecular adsorption or diffusion at a level that goes beyond a simple geometric description, the interatomic potentials that govern the adsorbate and the MOF framework must be specified. As in the results above, we assume that each MOF framework is rigid, and we consider the regime where the loading of the adsorbed molecule is low. Under these assumptions, only the interatomic potentials between the adsorbate and the MOF's framework atoms must be defined. We further limit our attention to nonpolar adsorbates, since this removes the necessity of assigning charges to each MOF framework atom, a time-consuming task that currently requires quantum chemistry calculations for each MOF that is considered.[23] We model CH_4-MOF interactions using the approach that has been used in multiple previous simulations of adsorption in MOFs[23−26] by defining a Lennard-Jones potential with parameters defined by mixing rules using the Lennard-Jones potentials for CH_4-CH_4 interactions and from the universal force field[27] for framework atoms. This approach fully defines the interatomic potentials needed for all MOFs without requiring any special fitting or parametrization for MOFs that have not been studied previously. The same approach can also be applied to other nonpolar spherical adsorbates.

We first consider the Henry's constant, which defines the slope of the adsorption isotherm in the limit of low pressures where the adsorbed amount is proportional to pressure. This quantity is a useful measure of a material's affinity for an adsorbate. The Henry's constant, K_H, of any spatially periodic material can be expressed in terms of integrals taken over a single unit cell:[28,29]

$$K_H\left(\frac{\text{mmol}}{\text{cm}^3\ \text{atm}}\right) = \frac{1}{RT}\frac{\int \exp(-\beta U^{\text{ads}})\mathrm{d}r^3}{\int \exp(-\beta U^{\text{ig}})\mathrm{d}r^3} \cong \frac{1}{RT}\frac{\sum_{i=1}^{N_{\text{points}}} \exp(-\beta U_i^{\text{ads}})}{N_{\text{points}}} \quad (1)$$

Here, U^{ads} and U^{ig} are the potential energy of a molecule in the adsorbed phase and the ideal gas phase, respectively, R is the ideal gas constant, and $\beta = 1/k_BT$. Because $U^{\text{ig}} = 0$ for a simple adsorbate, the integrals can be accurately approximated by the sum on the right-hand side above, where the summation is taken over a set of points covering the unit cell.

The Henry's constant for each MOF is calculated in conjunction with the pore size calculations described above. Those calculations define a set of grid points that span the unit cell of each MOF, along with the maximum hard sphere diameter that can be inserted at each grid point without overlapping any framework atoms. We evaluate the summation that defines the Henry's constant over the grid points for which the maximum hard sphere diameter is >1.5 Å. The very large positive values of U^{ads} associated with positions where the maximum hard sphere diameter was <1.5 Å mean that the contribution of these locations to the overall Henry's constant is negligible. The Henry's constant was calculated for CH_4 and H_2 for all the examined structures using a united atom model for both adsorbates with Lennard-Jones parameters that are shown in Table 1.

Table 1. Lennard-Jones Parameters (CH_4[29], CF_4[28], He,[46] Ne,[47] H_2[47], Ar,[46] Kr,[47] and Xe[47]) and the Range of Pore-Limiting Diameters Corresponding to the Range of Interest for Eight Spherical Adsorbates

	ε/k_B(K)	σ (Å)	d_{min} (Å)	d_{max} (Å)
CH_4	147.9	3.73	2.206	3.635
CF_4	134	4.66	2.839	4.391
He	10.9	2.64	0.856	2.221
Ne	35.7	2.789	1.164	2.517
H_2	38	2.9415	1.952	2.705
Ar	119.8	3.4	1.846	3.230
Kr	163.99	3.827	2.238	3.663
Xe	216.85	4.1	3.153	3.853

The calculation of the Henry's constant described above involves computing the total potential energy for the spherical adsorbate of interest at each grid point in the MOF. This information can also be used to rapidly estimate the net activation energy for diffusion of the molecule through the material. Although diffusion of molecules through a nanoporous material may involve multiple distinct energy barriers, it is the energy difference between the overall minimum energy state and the transition state with the highest energy that will control the overall diffusion rate. To make this estimate, we first identify the minimum energy state for the adsorbed molecule among all grid points within the major pore. We then consider the set of grid points at which the adsorbate energy lies within some interval, δE, of the energy minimum, and classify the connectivity of this set of points using the cluster analysis described earlier. If this set of grid points does not include (does include) a spanning cluster, then the activation energy for net diffusion of the adsorbate is smaller than (larger than) δE. Once two values of δE, one below and one above the actual activation energy, are known, a bisection algorithm can be used to rapidly determine an accurate value for the net activation energy of diffusion, ΔE_{diff}.

It is useful to adapt the information from the calculations above to predict the overall selectivity of MOFs as membranes. The ideal selectivity of a material in the Henry's regime for a pair of adsorbates can be estimated using[26]

$$S_{a/b} = \frac{C_a}{C_b}\frac{D_a}{D_b} \cong \frac{K_{h_a}\exp\left(-\frac{\Delta E_{\text{diff}_a}}{RT}\right)\sqrt{M_{r_b}}}{K_{h_b}\exp\left(-\frac{\Delta E_{\text{diff}_b}}{RT}\right)\sqrt{M_{r_a}}} \quad (2)$$

Here, C is the adsorbed concentration, D is the self-diffusivity, K_h is the Henry's constant, ΔE_{diff} is the diffusion energy barrier, and M_r is the molecular mass of an adsorbate. The right-hand side of this approximation assumes that the diffusivities can be expressed using a transition-state theory and that the pre-exponential factors associated with hopping over the rate-controlling barrier are of the same order of magnitude for both adsorbates. If the energy barriers for diffusion are negligible, the ratio of diffusivities used in this expression becomes that of Knudsen diffusion.

2.3. Estimation of Membrane Permeability. As mentioned above, one of the key applications of materials that accomplish

(23) Keskin, S.; Liu, J.; Rankin, R. B.; Johnson, J. K.; Sholl, D. S. *Ind. Eng. Chem. Res.* **2008**, *48*, 2355.
(24) Keskin, S.; Sholl, D. S. *Ind. Eng. Chem. Res.* **2009**, *48*, 914.
(25) Skoulidas, A. I.; Sholl, D. S. *J. Phys. Chem. B* **2005**, *109*, 15760.
(26) Keskin, S.; Sholl, D. S. *Langmuir* **2009**, *25*, 11786.
(27) Rappe, A. K.; Casewit, C. J.; Colwell, K. S.; Goddard, W. A.; Skiff, W. M. *J. Am. Chem. Soc.* **1992**, *114*, 10024.
(28) June, R. L.; Bell, A. T.; Theodorou, D. N. *J. Phys. Chem.* **1990**, *94*, 1508.
(29) Goodbody, S. J.; Watanabe, K.; MacGowen, D.; Walton, J. P. R. B.; Quirke, N. *J. Chem. Soc., Faraday Trans.* **1991**, *87*, 1951.
(30) Keskin, S.; Liu, J.; Johnson, J. K.; Sholl, D. S. *Microporous Mesoporous Mater.* **2009**, *125*, 101.

kinetic separations is in membranes. Detailed models of the performance of MOFs as membranes are available,[26,30] but in the Henry's regime, membrane performance can be estimated using the quantities described above. The net permeability of a species passing through a membrane defined as

$$\Pi = \frac{J}{\Delta P/L}\left(10^{-10}\frac{\frac{\mathrm{cm}^3_{\text{ideal gas}}}{\mathrm{s\ cm}^2}}{\mathrm{cmHg/cm}} = \frac{10^{-10}\ \mathrm{cm}^3\ \mathrm{cm}}{\mathrm{cm}^2\ \mathrm{s\ cmHg}}\ \text{or Barrer}\right) \quad (3)$$

where J is the flux the membrane, ΔP is the pressure drop across the membrane, and L is the membrane thickness. Within Henry's regime, the flux can be expressed as

$$J = -D\frac{\Delta C}{L} = -DK_h\frac{\Delta P}{L} \quad (4)$$

which gives $\Pi = DK_h$, where D is the diffusivity and K_h is the Henry's constant. The diffusivity can be estimated by a transition state description[7,31] as $D = ka^2/2$, where k is the hopping rate over the rate-controlling barrier and a is the distance that is covered during the hopping. The hopping rate can be expressed as $k = \nu \exp(-\Delta E_{diff}/RT)$, where the pre-exponential factor ν is assumed to be 10^{12}. For simplicity, we assume that for all structures the distance covered with one hop is $a = 10$ Å. These assumptions are discussed further in section 3.3.

3. Results and Discussion

3.1. Comparison with Previous Work for Silica Zeolites. The geometrical methods described above are similar to the previous work of Foster et al. on the pores in silica zeolites.[10] In that work, the Delaunay triangulation method was used to extract the largest cavity diameter and the pore-limiting diameter for 165 silica zeolite frameworks. To validate our calculations, we applied our method to the same set of 165 materials. For each zeolite, we obtained the crystal structure from the IZA Zeolite Database[32] and performed the calculations defined above with a grid spacing of 0.1 Å.

Our results for silica zeolites are summarized in Figure 2. In general, the agreement between our calculations and the earlier results of Foster et al. is excellent. There are three cases in which the largest cavity diameter we calculated and the previous report differ by almost 0.5 Å. We suspect, but are unable to confirm, that this stems from slight differences in the crystal structures used in these two sets of calculations. A more interesting point is that for two structures, the zeolite frameworks RUT and AFN, our calculation gives a noticeably larger pore-limiting diameter than was reported by Foster et al. This occurs because Foster et al. only considered pores oriented along the material's crystallographic axis. In these two materials, the pores that define the pore-limiting diameter are not oriented along one of these directions. Finally, we found that for five zeolite frameworks (BCT, CGF, FER, MWW, and RSN) the largest cavity diameter reported by Foster et al. does not fall within the major channel as defined above. That means that the reported cavity is not accessible to a probe sphere of size equal to the pore- limiting diameter. This situation is illustrated for FER in Figure 3. In this zeolite, the major channel is oriented along the [001] direction with a pore-limiting diameter of 4.628 Å. The global result for the largest cavity diameter (6.250 Å) is shown as a yellow sphere in Figure 3, but only probe spheres with radii smaller than 3.325 Å can pass between this cavity and the major channel without overlapping framework atoms. If we restrict our attention to the largest cavity size that is accessible within the major channel, the largest cavity in FER is 5.543 Å, which is 0.7 Å smaller than the yellow sphere shown in Figure 3. In order to facilitate a comparison between our calculations and the results of Foster et al., Figure 2 uses the global largest cavity diameter for all 165 zeolites.

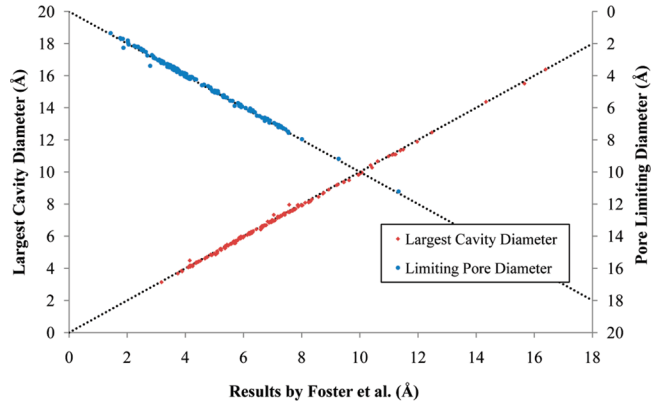

Figure 2. Calculated largest cavity diameter (left axis) and pore-limiting diameter (right axis in reverse order) for 165 silica zeolites compared with the results reported by Foster et al. Dotted lines show the situation where our calculations and the results of Foster et al. agree exactly.

A simplifying feature of silica zeolites is that the interiors of all pores in these materials are defined by O atoms. For this reason, a geometric analysis of the pore structure can be performed without needing to define the sizes of different atomic species. This simplification makes the use of Delaunay triangulation more straightforward for these chemically simple pores than it would be for the chemically richer structures defined by MOFs. Because the method we have defined above provides a natural way to describe pores comprised of arbitrary atomic species, our method is better suited to examining MOFs than the methods of Foster et al.

3.2. Pore-Limiting Diameters and Largest Cavity Diameters of MOFs. To demonstrate the value of our methods for characterizing MOFs, we examined the collection of 774 MOFs compiled in 2005 by Ockwig et al.[33] This list was originally developed to perform a taxonomical analysis of the types of topological nets that occur in MOFs.[33] Although the number of known MOF structures continues to grow rapidly, this collection of structures defines a useful benchmark for our approach because it spans a wide range of structural motifs. For each MOF, the coordinates of the framework atoms were defined from the experimentally reported crystal structures after removing any solvent molecules from the reported structure. For ionic frameworks the counterions were considered part of the framework and were not removed. For many structures, the crystal structure available from the CSD either does not have the same stoichiometry as the true material due to missing atoms (typically H) or exhibits a considerable degree of disorder. A number of structures were corrected manually, but we do not report results for 269 materials with these characteristics below. In addition, five of the structures listed by Ockwig et al. are not available in the Cambridge Structural Database, so we did not examine these materials. Moreover, we examined four MOFs

(31) Ford, D. M.; Glandt, E. D. *J. Phys. Chem.* **1995**, *99*, 11543.
(32) Baerlocher, Ch.; McCusker, L. B. *Database of Zeolite Structures*. http://www.iza-structure.org/databases/ (accessed May 5, 2010).
(33) Ockwig, N. W.; Delgado-Friedrichs, O.; O'Keeffe, M.; Yaghi, O. M. *Acc. Chem. Res.* **2005**, *38*, 176.

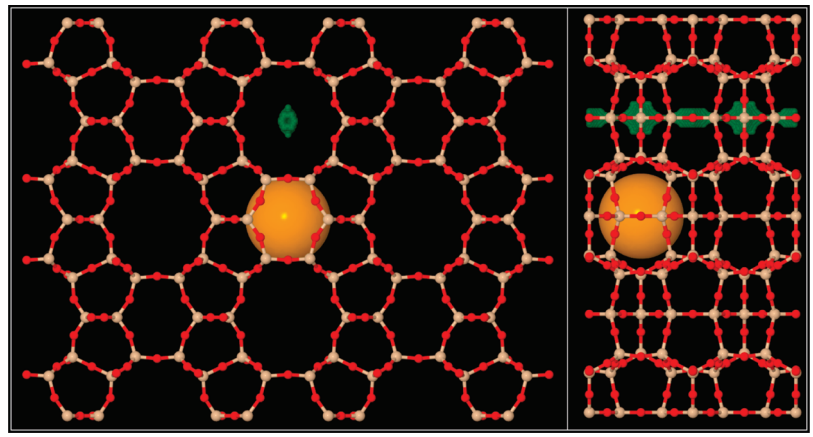

Figure 3. Graphical representation of the zeolite FER viewed along [001] (left) and [100] (right). The framework atoms are colored red (O) and beige (Si). The largest cavity present in the structure is represented as a yellow sphere a diameter of 6.250 Å. The green points represent the coordinates that are accessible to a hard sphere of diameter equal to the pore-limiting diameter of 4.628 Å.

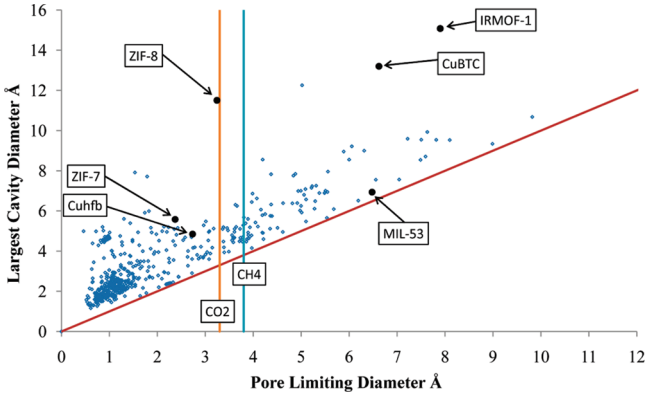

Figure 4. Values for the largest cavity diameter and pore-limiting diameter for 504 MOF structures. The kinetic diameters of CO_2 and CH_4 are shown with black vertical lines. The red line shows the extreme case for which the pore-limiting diameter is equal to the largest cavity diameter.

structures not included in Ockwig et al.'s list for which efforts at membrane fabrication have been reported. These additional materials are CuBTC (in its fully dehydrated form), ZIF-7, ZIF-8, and Cu(hfipbb)$(H_2$hfipbb$)_{0.5}$.[8,34−36] This procedure gave a total of 504 distinct structures with unit cells that varied in volume from 269 to 70539 Å^3. We reiterate that our calculations were performed while holding all framework atoms rigid in the experimentally reported structure.

The calculated pore-limiting diameter and largest cavity size for the 504 MOFs we have considered are summarized in Figure 4. A large number of these materials are seen to be essentially nonporous, with pore-limiting diameters smaller than 2 Å. Most of these structures are ionic frameworks that have counterions present in their pores. At the other extreme, several materials with pore-limiting diameters approaching 10 Å exist. ~86% of the MOFs have largest cavity sizes that are ≤2.5 Å larger than the pore-limiting diameter. In a small number of examples, the largest cavity size and the pore-limiting diameter are essentially equal. An example of a material of this kind is MIL-53, which is illustrated in Figure S1 in the Supporting Information. In MIL-53, the pores are shaped by the BDC linkers which are aligned in such a way that the direction of the channel runs along the plane of the linkers. These linkers form a channel with an almost constant inner diameter. In contrast, a number of materials have largest cavity sizes that are much larger than the pore-limiting diameter. One example of this is the well-known material IRMOF-1, which is shown in Figure S1 in the Supporting Information. This MOF has a cavity size that is 7 Å greater than the pore-limiting diameter. A list of 25 materials that sample the range of the materials we have considered together with their calculated pore characteristics is given in the Supporting Information.

A useful, albeit simplistic, way to use the data in Figure 4 to select materials that may have value for kinetic separations is to compare the calculated pore-limiting diameters with the kinetic diameters of diffusing molecules. Kinetic diameters are typically derived by fitting second virial coefficient data to an empirical interatomic potential.[37] These quantities become less meaningful as the shape and size of molecules increases, but they are nevertheless valuable for heuristically understanding the implication of Figure 4. As an example, we indicate in Figure 4 the kinetic diameters of CO_2 and CH_4.[37] There is significant industrial interest in separating these two similarly sized molecules because of the large volumes of CO_2-contaminated natural gas that are known globally.[38] Superimposing the kinetic diameters in Figure 4 immediately provides useful guidance about which MOFs could potentially be used for high selectivity kinetic separations of CO_2 and CH_4. Materials that have pore-limiting diameters considerably larger than the kinetic diameter of CH_4 are likely to allow both species to diffuse rapidly through their pores, meaning that at best a moderate level of selectivity based on molecular diffusion can be attained. This qualitative conclusion has been borne out in a range of more detailed modeling studies of gas diffusion and separation in large pore MOFs.[24,26] On the other hand, materials with pore-limiting diameters substantially smaller than the kinetic diameter of CO_2 will not allow either molecule to permeate through a MOF crystal, so these materials would be of little value in separations applications.

(34) Chui, S. S.-Y.; Lo, S. M.-F.; Charmant, J. P. H.; Orpen, A. G.; Williams, I. D. *Science* **1999**, *283*, 1148.
(35) Wu, H.; Zhou, W.; Yildirim, T. *J. Am. Chem. Soc.* **2007**, *129*, 5314.
(36) Park, K. S.; Ni, Z.; Côte, A. P.; Choi, J. Y.; Huang, R.; Uribe-Romo, F. J.; Chae, H. K.; O'Keeffe, M.; Yaghi, O. M. *Proc. Natl. Acad. Sci. U.S.A.* **2006**, *103*, 10186.
(37) Breck, D. W. *Zeolite Molecular Sieves: Structure, Chemistry, and Use*: John Wiley & Sons, Inc.: New York, 1974.
(38) Kidnay, A. J.; Rarrish, W. R. *Fundamentals of Natural Gas Processing*; CRC Press: Boca Raton, 2006.

Figure 4 highlights five materials for which membrane fabrication has been attempted:[39−44] IRMOF-1, CuBTC, ZIF-7, ZIF-8, and Cu(hfipbb)(H_2hfipbb)$_{0.5}$. The latter material is denoted Cuhfb on the figure. IRMOF-1 and CuBTC have values of the pore-limiting diameter larger than 6 Å and, therefore, are not expected to result in high selectivity values for separating small molecules such as CH_4, CO_2, and H_2. The two ZIF materials and Cu(hfipbb)(H_2hfipbb)$_{0.5}$, however, have pore-limiting diameter values between 2 and 4 Å. This range is comparable with the molecular diameters of small molecules and suggests that these materials are interesting candidates for kinetic separations. It is also worth noting the considerable difference between the largest cavity diameter and the pore-limiting diameter for ZIF-8, which has cages of diameter 11.5 Å connected via windows of diameter 3.2 Å.

It is important to note that the use of kinetic diameters outlined above cannot be taken literally. Real molecules are not simply spherical hard spheres. For approximately spherical adsorbates such as CH_4, pores with pore-limiting diameters slightly smaller than the molecule do not define an infinitely high energy barrier to molecular diffusion. Instead, an energy barrier of finite height will control molecular diffusion, with the height of this barrier depending on the details of the repulsive interactions between the adsorbate and framework. A good example of this idea is the MOF Cu(hfipbb)(H_2hfipbb)$_{0.5}$, which was recently considered for CO_2/CH_4 separations using a combination of molecular modeling and quantum chemistry calculations by Watanabe et al.[9] The pore-limiting diameter of Cu(hfipbb)(H_2hfipbb)$_{0.5}$ as defined by our methods is 2.735 Å. This is smaller than the nominal kinetic diameter of CO_2 (CH_4) by 0.565 (1.065) Å. If the kinetic diameters shown in Figure 4 were interpreted naively, this MOF would not be considered as an interesting candidate for CO_2/CH_4 separations. When an interatomic forcefield based on the universal force field (UFF), however, was used to characterize CH_4 motion along the one-dimensional pores of Cu(hfipbb)(H_2hfipbb)$_{0.5}$ in calculations that held the framework in a fixed geometry, it was found that CH_4 could diffuse in this material by overcoming an energy barrier of ~70 kJ/mol between adjacent cavities in the pore.[9] Quantum chemistry calculations that allowed framework flexibility indicated that this flexibility reduced this barrier somewhat, although the resulting barrier was still large. In contrast, CO_2 experiences an energy barrier to diffusion in the same material of ~10 kJ/mol and is therefore able to diffuse far faster than CH_4. That is, both molecules can diffuse through this MOF, but at enormously different rates. This is precisely the situation that is desirable for a material used in a kinetically based separation.

The example we just described indicates that kinetic diameters can be used to identify materials with interesting diffusion properties provided that a range of pore-limiting diameters around the nominal kinetic diameters are considered. As a specific example, a reasonable way to consider the data in Figure 4 for kinetic separations of CO_2/CH_4 mixtures would be to exclude all structures that have pore-limiting diameters smaller than 2 Å or larger than 4 Å. We have replotted our data to highlight the materials that fulfill these criteria in Figure 5. This analysis yields 104 materials that can be considered further for this separation, and, just as importantly, excludes 400 materials that are highly unlikely to have useful properties for this application. ZIF-7, ZIF-8, and Cu(hfipbb)(H_2hfipbb)$_{0.5}$, as mentioned above, fall within the useful range and have been labeled in Figure 5. The ability to characterize large numbers of materials and to efficiently exclude a large fraction of them from further consideration is crucial when attempting to identify new materials for specific applications, so this kind of calculation should find numerous uses for a variety of chemical separations. Once a set of candidate materials has been identified for an application of interest, it is important to be able to move beyond the purely geometric analysis we have considered to this point and perform a more detailed analysis. In the next section, we show how the methods we have already described make it possible to achieve this goal in an efficient way by enabling a more detailed description of the adsorption and diffusion characteristics of simple molecules in MOFs.

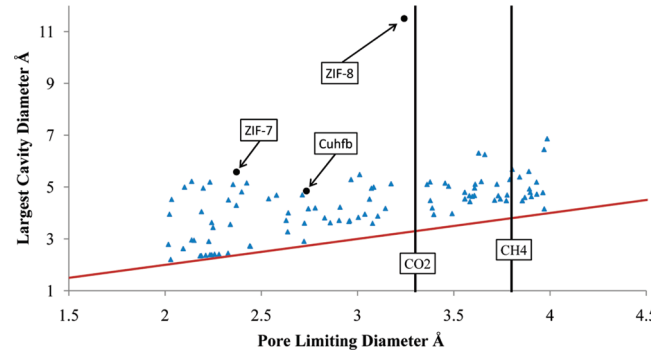

Figure 5. Values of the largest cavity diameter and pore-limiting diameter for 101 MOF structures with pore-limiting diameter between 2 and 4 Å. The kinetic diameters of CO_2 and CH_4 are shown with vertical lines.

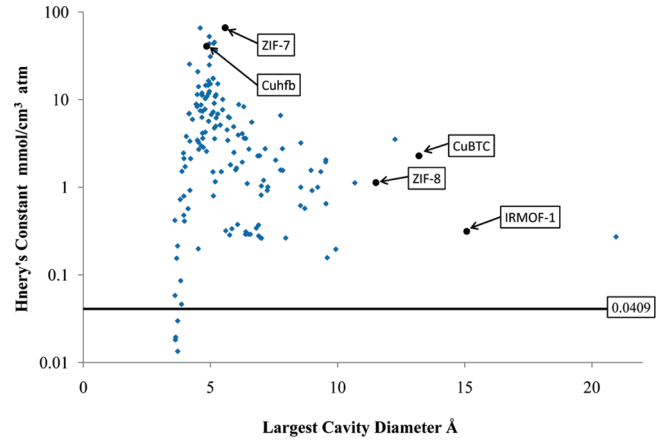

Figure 6. Calculated Henry's constant for CH_4 at 298 K as a function of the largest cavity diameter for 152 MOFs satisfying the criteria listed in the text. The horizontal line represents the equivalent of the Henry's constant for an ideal gas.

3.3. Henry's Constant and Diffusion Barrier for Spherical Adsorbates. We illustrate the Henry's constant calculations for CH_4 at 298 K for 152 MOFs in Figure 6. For all of the remaining MOFs from the 504 structures introduced above, the Henry's constant was calculated to be less than 0.01 mmol/cm^3/atm, and/or the diffusion barrier for CH_4 (estimated as described below)

(39) Bux, H.; Liang, F.; Li, Y.; Cravillon, J.; Wiebcke, M.; Caro, J. *J. Am. Chem. Soc.* **2009**, *131*, 16000.
(40) Guo, H.; Zhu, G.; Hewitt, I. J.; Qiu, S. *J. Am. Chem. Soc.* **2009**, *131*, 1646.
(41) Li, Y.-S.; Liang, F.-Y.; Bux, H.; Feldhoff, A.; Yang, W.-S.; Caro, J. *Angew. Chem., Int. Ed.* **2010**, *49*, 548.
(42) Liu, Y.; Ng, Z.; Khan, E. A.; Jeong, H.-K.; Ching, C.-B.; Lai, Z. *Microporous Mesoporous Mater.* **2009**, *118*, 296.
(43) Ranjan, R.; Tsapatsis, M. *Chem. Mater.* **2009**, *21*, 4920.
(44) Yoo, Y.; Lai, Z.; Jeong, H.-K. *Microporous Mesoporous Mater.* **2009**, *123*, 100.

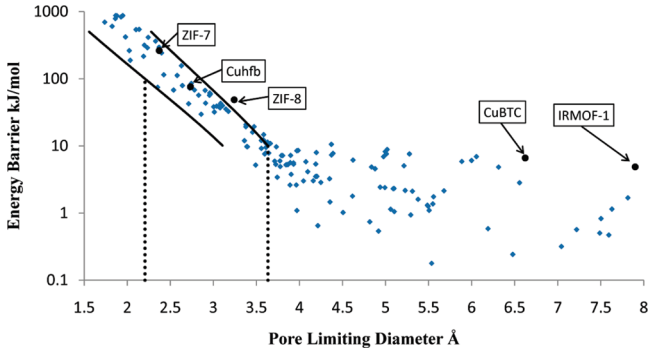

Figure 7. Calculated energy barrier for CH_4 diffusion in 216 MOFs shown as a function of the pore-limiting diameter. The solid lines are the upper and lower bounds on the energy barrier described in the text.

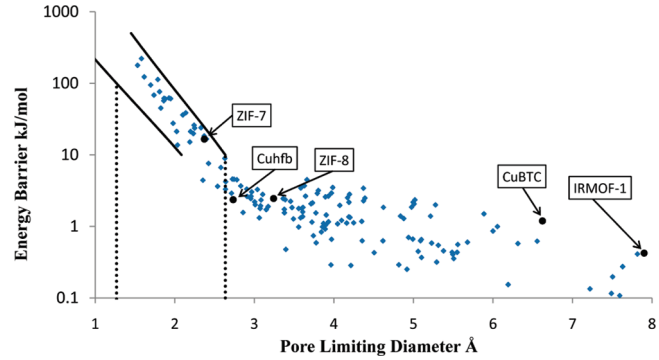

Figure 8. Calculated energy barrier for H_2 diffusion in 216 MOFs shown as a function of the pore-limiting diameter. The solid lines are the upper and lower bounds on the energy barrier described in the text.

was larger than 1000 kJ/mol. In other words, CH_4 cannot adsorb to any appreciable extent in the MOFs not shown in Figure 6. The horizontal solid line in the figure represents a volume that is empty apart from an ideal gas. Structures with Henry's constants above this line can increase the overall density of CH_4 (in the Henry's law regime) relative to an ideal gas.

For MOFs with largest cavity sizes up to the size of a CH_4 molecule, roughly 4 Å, a strong correlation exists between the cavity size and the Henry's constant. In these instances, interactions between the adsorbed molecule and the MOF are dominated by the repulsive part of the pair potentials. When larger cavities are present, positions exist for the adsorbate that reduce the repulsive interactions and thus result in higher values of K_H. The largest Henry's constant we observe are for structures with a largest cavity diameter of approximately 5 Å. One such example is the structure with Refcode MIMVEJ ($[Zn(nicotinate)_2]_n$)[45] which has straight channels with a largest cavity diameter of 4.599 Å. These high Henry's constants can be attributed to the fact that in the middle of such a cavity a CH_4 molecule can obtain a position that achieves the maximum positive interactions with all surrounding framework atoms. A graphical representation of this material can be seen in Figure S2 in the Supporting Information. For MOFs with cavities larger than this, the overall Henry's constant is not well correlated with the largest cavity size.

Figure 7 shows the values of the diffusion activation energy defined in section 2.2 as a function of the pore-limiting diameter for the 156 structures whose Henry's constants were described earlier in this section. This set of materials excludes (from the 504 materials we examined) any MOF with a calculated energy barrier for diffusion greater than 1000 kJ/mol. For MOFs whose pore-limiting diameter is comparable or smaller to the diameter of CH_4, a strong correlation exists between the pore-limiting diameter and the calculated activation energy for diffusion. This observation is not surprising; as the pore-limiting diameter becomes smaller than the size of a diffusing molecule, a strong overlap with the framework atoms is created at the bottleneck of the pore. A similar correlation does not exist between the activation energy for diffusion and the largest cavity diameter, since the size of the largest cavity does not control net diffusion as long as it is large enough for the diffusing molecule to adsorb readily. The activation energy has been plotted for H_2 in Figure 8 against the pore-limiting diameter for 165 MOFs using the same criteria for the range of Henry's constants and energy barrier values as in Figure 7. For the large pore materials in Figures 7 and 8 the activation energies are small but show a significant degree of variation. This variation exists because the energy barrier is the difference between the energy at the position of the pore-limiting diameter and the global energy minimum. The former energy is strongly correlated with the pore-limiting diameter, but the latter energy is not.

The connection between the pore-limiting diameter and the diffusion activation energy can be used to place useful bounds on the activation energy that are independent of the specific details of the MOF structure. To define these bounds, we assume that the pore-limiting diameter defines the relevant transition state for net diffusion and that the potential energy at this location is a result of only the overlap with the adsorbate molecule with a number of framework atoms that create the bottleneck of the pore. We also assume that the potential energy at the energy minimum in the pore is negligible relative to the energy at the transition state. We then calculate the potential energy of an adsorbate molecule being in the center of a circular pore bottleneck as a function of the diameter of the bottleneck. For the lower (upper) bound it is assumed that the hypothetical bottleneck is defined by two C (four H) atoms. This description was chosen to capture the features of the data in Figure 7 but is based on plausible approximations of the environment likely to exist in most MOFs. The two solid lines in Figure 7 show the resulting bounds for the diffusion activation energy of CH_4 in MOFs, where it can be seen that they accurately capture the trends observed in our more detailed calculations for all MOFs with pore-limiting diameters similar in size or smaller than the size of a CH_4 molecule. These bounds are also shown in Figure 8, where they were calculated using the same description and the Lennard-Jones parameters for H_2. The bounds also give a useful estimate of the activation energies for this adsorbate.

An immediate use for the approximate bounds on the diffusion activation energy just introduced is to define a range of MOFs for which significant diffusion limitations will exist for an adsorbed molecule while still allowing diffusion at experimentally observable rates. We did this by determining the range of pore-limiting diameters based on our upper and lower bounds. The lower value for this range was chosen to be the value where the lower bound for the diffusion activation energy was 100 kJ/mol. Any MOF with a pore-limiting diameter smaller than this value will have a diffusion activation energy

(45) Rather, B.; Moulton, B.; Walsh, R. D. B.; Zaworotko, M. J. *Chem. Commun.* **2002**, 694.
(46) Maitland, G. C. R. M. Smith, E. B.; Wakeham, W. A. *Intermolecular Forces: Their Origin and Determination*; Clarendon Press: Oxford, U.K., 1981.
(47) Hirschfelder, J. O.; Curtiss, C. F.; Bird, R. B. *Molecular Theory of Gases and Liquids*; Wiley: New York, 1965.

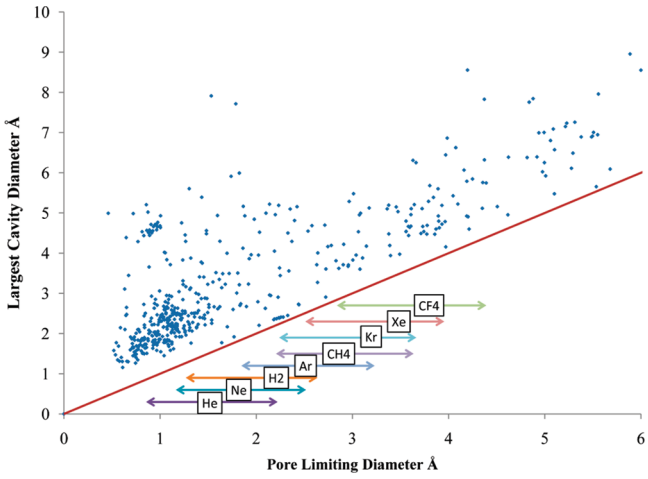

Figure 9. Values of the largest cavity diameter and pore-limiting diameter for 504 MOF structures. The arrows on the bottom part of the graph represent the range of interest for eight spherical adsorbates as determined using the methods in the text.

larger (possibly far larger) than 100 kJ/mol. The upper value for this range was defined by the pore-limiting diameter for which the upper bound defined above was 10 kJ/mol. These numerical values are of course somewhat arbitrary, but they give a useful means of refining the concept of the size of a diffusing molecule relative to the MOF structure. Applying this analysis for CH_4 predicts that MOFs with pore-limiting diameters between 2.2 and 3.6 Å will define significant diffusion activation energies. This entire range of diameters is smaller than the kinetic diameter of CH_4 mentioned above (3.8 Å), and this analysis accounts for the observation that Cu(hfipbb)-$(H_2hfipbb)_{0.5}$ is an interesting material in terms of its properties for CH_4 diffusion even though its pore-limiting diameter is smaller than the kinetic diameter of CH_4.

One powerful conclusion of this analysis is that we can now make useful predictions about the diffusion activation energies for a large range of spherical adsorbates in a large range of MOFs without performing detailed calculations for each adsorbate in each MOF. To do so, we assign a range of pore-limiting diameters for each adsorbate based on the bounds associated with the pore-limiting diameters for the complete set of MOFs we have considered. This result is summarized visually in Figure 9, where we indicate the range of MOFs that will create significant diffusion barriers for CH_4, He, Ne, Ar, Kr, Xe, H_2, and CF_4. Each molecule was represented by a spherical molecule with the Lennard-Jones parameters listed in Table 1.[28,29,46,47] This analysis provides an efficient means of identifying MOFs that would be of potential interest for achieving kinetic separations of molecules that are similar in size.

Figure 10 shows the estimated ideal selectivity based on eq 2 for H_2 over CH_4 at 298 K for 134 of the 504 MOFs we have considered. We have not included in this plot materials that are unable to accommodate H_2 (K_h < 0.01 mmol/cm^3/atm) or structures with a energy barrier for CH_4 diffusion >300 kJ/mol. Two distinct regimes can be identified in this figure, one limited by adsorption and one by diffusion. In the adsorption limited regime the selectivity favors CH_4 due to the stronger dispersion interactions with the framework. Within this regime, maximum selectivity toward CH_4 is observed for pore sizes around 5 Å for which, as explained before, the CH_4 can maximize its interactions with the surrounding atoms. In the diffusion limited regime, the selectivity favors the smaller molecule (H_2). In this regime, the estimated selectivity becomes extremely large as the pore-limiting diameter is reduced and the diffusion energy barrier for CH_4 increases. The fact that large selectivities like this can exist within the approximations we have used is not in itself surprising; the value of these calculations is that they efficiently show which materials can potentially have this property.

3.4. Permeability of MOF Structures. As described in section 2.3, it is possible to use our results to predict the permeability of a gas through a MOF crystal. These predictions are most directly applicable to membranes grown from thin films of MOFs,[24,30] but this information is also needed to consider MOFs as minority components in polymer/MOF composite membranes.[48] For simplicity, we estimated the hopping distance and pre-exponential factor to be 10 Å and 10^{12} s^{-1}, respectively. These estimates could be refined if a detailed model of a particular MOF was needed, but such a refinement will not change the qualitative outcome given by our simpler approach. For IRMOF-1, our estimate predicts a H_2 permeability of 3.17 $\times$ 10^5 Barrer, which compares well to results from detailed molecular modeling[24] that gave 2.99 $\times$ 10^5 Barrer.

Our calculated H_2 permeability and H_2/CH_4 ideal selectivity for a large collection of MOFs is summarized in Figure 11. This figure also includes the well-known upper bound curve for polymeric membranes compiled from extensive experimental data by Robeson.[49] The solid line in the figure indicates Robeson's upper bound in the regime where polymeric membranes have been demonstrated, while the dashed line extrapolates the upper bound to higher permeabilities. A large number of MOFs are predicted to have H_2 permeability far higher than is available with any known polymer while having only moderate selectivity for H_2/CH_4. This group includes IRMOF-1 and CuBTC.

The most striking feature of Figure 11 is the collection of MOFs that are predicted to have high permeability relative to known polymers *and* extraordinarily high selectivity. This group of materials includes ZIF-8 and Cu(hfipbb)$(H_2hfipbb)_{0.5}$ (labeled Cuhfb on the figure). For these materials, our calculations predict that an extremely selective kinetic separation is possible, as already seen in Figure 10. In polymeric membranes, large increases in membrane selectivity are closely correlated with large decreases in permeability; this is the trade-off encapsulated by Robeson's upper bound. In contrast, our calculations predict that extremely high permeability is possible with MOF crystals even when the crystal structure is expected to give very high selectivity.

The same set of calculations described above were also carried out for all the 191 pure silica zeolite frameworks currently found in the zeolite database.[32] For this case the interactions between the framework and the adsorbates were determined by using the Lennard-Jones parameters shown in Table 2 that have been developed for zeolites and have been used in previous molecular simulation studies.[50,51] The results for the selectivity and permeability are also shown Figure 11. From this figure it can be observed that the zeolite frameworks behave in a qualitatively similar way to the MOF structures. Most of the zeolites are scattered across a range of low selectivities with high permeabilities, and a small number with appropriate pore-limiting

(48) Keskin, S.; Sholl, D. S. *Energy Environ.* **2010**, *3*, 343.
(49) Robeson, L. M. *J. Membr. Sci.* **1991**, *62*, 165.
(50) Skoulidas, A. I.; Sholl, D. S. *J. Phys. Chem. B* **2002**, *106*, 5058.
(51) Akten, E. D.; Siriwardane, R.; Sholl, D. S. *Energy Fuels* **2003**, *17*, 977.

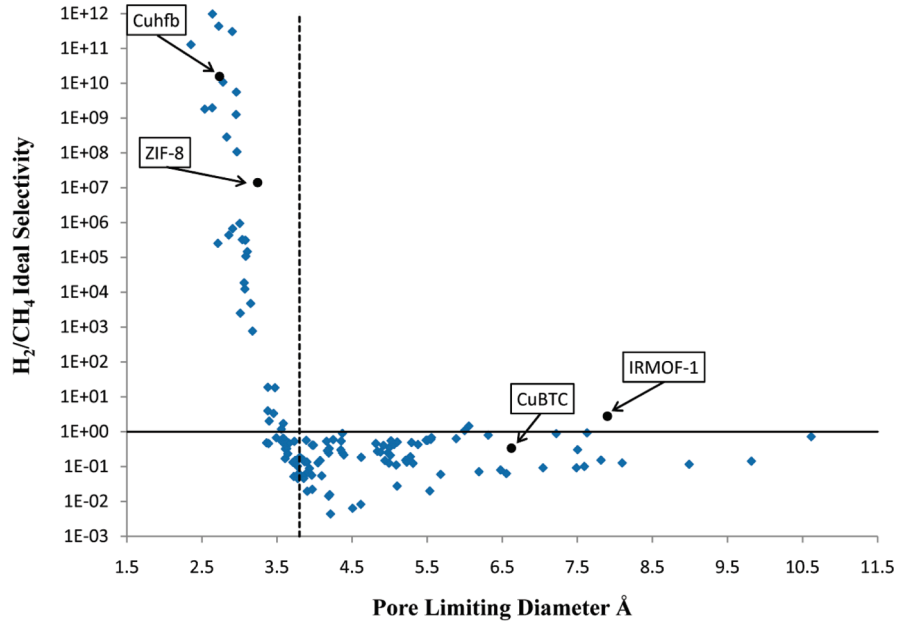

Figure 10. Calculated ideal selectivity within Henry's regime for H_2/CH_4 for 143 MOF structures at 298 K as a function of the pore-limiting diameter. The horizontal solid line indicates a nonselective material. The dashed vertical line represents the kinetic diameter of CH_4.

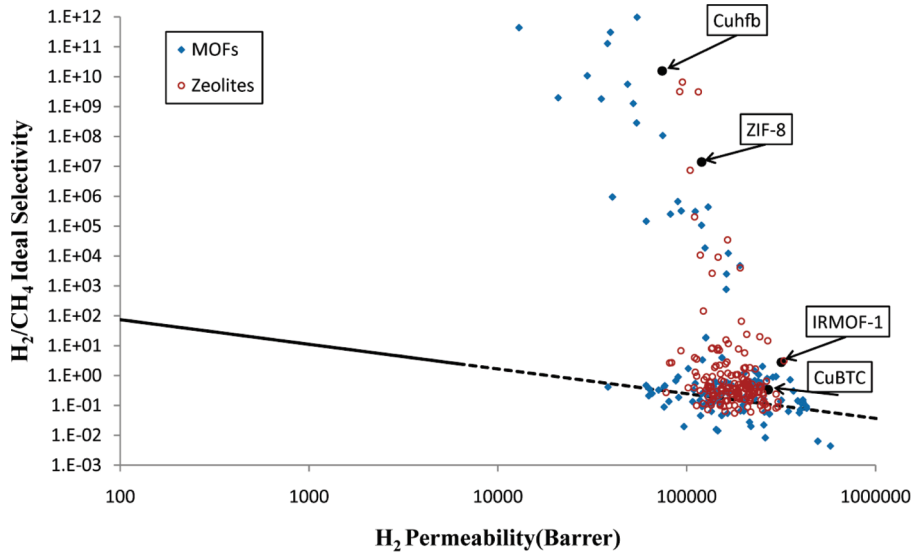

Figure 11. Calculated H_2/CH_4 ideal selectivity and H_2 permeability within Henry's regime for 143 MOF structures (filled symbols) and 191 zeolites (unfilled symbols) at 298 K. The solid line is Robeson's upper bound for H_2/CH_4 separations with polymeric membranes, including an extrapolation of this upper bound to high permeabilities shown as a dashed line.

Table 2. Lennard-Jones Values for CH_4[50]–Zeolite and H_2[51]–Zeolite Interactions

	ε/k_B(K)	σ (Å)
O_{zeo}-CH_4	133	3.214
O_{zeo}-H_2	72	2.708

diameters have very large selectivity. It should be noted that only a fraction of these zeolite frameworks have been synthesized successfully in the pure silica form that was modeled here.

3.4.1. Comparison with Experimental Data. Figures 10 and 11 highlight several MOFs for which experimental efforts to fabricate thin film membranes have been reported. Here, we compare our predictions with the available experimental data for these materials. For IRMOF-1 thin films,[42,44] H_2/CH_4 selectivities comparable to Knudsen diffusion selectivity (~2.8 for H_2/CH_4) have been observed experimentally. For CuBTC,[40] an ideal selectivity of 7.8 has been reported for H_2/CH_4. For ZIF-8 thin films,[39] a selectivity of a 1:1 H_2/CH_4 mixture was measured to be 11.2, whereas for ZIF-7 thin films[41] this value was found to be 5.9. For Cuhfb, no CH_4 permeation measurements have been reported. For a mixture of H_2/N_2, however, the selectivity was found to be 23 with a very low permeance.[43] It is important to note that these experiments measure the apparent selectivity of the grown membrane, which might be quite different from the intrinsic selectivity of the material due to defects associated with the microstructure in intergrown MOF layers. This challenge in interpreting results from thin films of intergrown crystals is well-known from past studies of zeolite membranes.[52,53]

For IRMOF-1, our predicted ideal selectivity (2.78 in the Henry's regime) is in good agreement with the experimental values. For CuBTC, our calculations predict an ideal selectivity that favors CH_4 by a factor of ~3. This is in agreement with recent detailed molecular modeling results[24] that predict small mixture selectivity values favoring CH_4 for a range of pressures. Experimentally, however, low selectivities favoring H_2 are observed. One puzzling aspect of these experiments is that at room temperature, H_2 is reported to adsorb more strongly than N_2. It would be helpful if further experimental data from films of this kind was available in order to probe the discrepancy between the existing observations and our predictions.

The differences between our predictions for ZIF-7 and ZIF-8 and experimental data from thin films of these materials are very large. Our calculations predict extremely high H_2/CH_4 selectivities for these two materials; ZIF-7 does not even appear in Figure 10 because of the range of selectivities we chose to include. These predicted selectivities are orders of magnitude larger than the modest selectivities that have been seen experimentally. We believe, although we cannot unambiguously demonstrate, that this discrepancy is mostly associated with defects in the microstructure of the intergrown thin films, where defects associated with grain boundaries can allow significant fluxes of CH_4 (and H_2) through the membranes. As mentioned above, assessing the relative contributions from flux through crystalline nanopores and flux through microstructural defects has been a significant challenge for many years in the development of thin film zeolite membranes. It is likely that this issue will also be a critical one in the newly developing area of thin film MOF membranes. The very low permeance observed with the one Cuhfb membrane that has been reported also suggests that the properties of this particular device were dominated by microstructural issues rather than the intrinsic diffusion of molecules inside the pores of Cuhfb. The fact that this MOF has one-dimensional pores provides a hint that controlling the orientation of MOF crystals within an intergrown film may be critical to the success of such a film as a membrane.

An alternative experimental strategy for examining the properties of MOFs for kinetic separations is to fabricate polymer/MOF composites in which MOF particles are the minority phase. These so-called mixed matrix membranes also come with practical challenges, since good adhesion between MOF particles and the polymer is necessary and it must be possible to readily disperse the polymer in the polymer matrix. A number of experiments have been performed using this approach but a different type of inorganic material.[54,55] Keskin and Sholl have recently introduced methods to model these composite membranes by combining experimental data from pure polymer films with predictions for MOF properties from molecular simulations.[48] These models showed quantitative agreement with the observed light gas permeability of IRMOF-1/Matrimid composites. As mentioned above, the simplified models we have introduced here predict gas permeability through IRMOF-1 in close agreement with more detailed molecular models. It is therefore possible for IRMOF-1 to compare experimental data from thin MOF films and polymer/MOF composites with modeling data, and in both cases, the modeling results and experiments are in close agreement. This suggests that the use of mixed matrix membranes may be a useful way to complement studies of thin film MOF membranes for other MOFs in order to attempt to understand the relative effects of microstructural defects and intrinsic crystalline properties in the latter devices.

We do not claim that our predictions are absolutely precise; we have clearly made a series of approximations regarding the nature of the MOFs we have studied. However, our predictions regarding ZIF-7, ZIF-8, and the other high-selectivity materials we have identified are sufficiently robust to motivate careful study of these materials with more precise methods, both theoretically and experimentally. In this same vein, our calculations have identified a large number of MOFs, including IRMOF-1 and CuBTC, that are of limited interest for kinetic separations of light gases. We view the methods we have introduced here as a valuable tool for screening materials at this "go/no-go" level in order to efficiently focus available resources on the materials that can have the most valuable properties. Any screening effort of this kind must ultimately be coupled with additional efforts to examine a small number of the most promising materials in a detailed way.

4. Conclusion

We have introduced efficient methods for describing the features of MOFs that control molecular diffusion in these materials. By examining over 500 MOFs, we have shown that these methods can be useful in identifying materials that are suitable for kinetic separations of adsorbed molecules. In addition to a geometric characterization of each MOF, our calculations rapidly predict the Henry's constant for adsorption and diffusion activation energy of simple gases. We expect that these methods will be a powerful tool for focusing attention on the materials that are best suited for applications of MOFs in molecular separations.

In any effort to use modeling in screening large numbers of materials, it is vital to clearly describe the limitations of the approach.[56] Perhaps the strongest assumption in our geometric characterization is that the MOF framework is rigid in its reported crystallographic structure. This assumption is clearly not correct in all cases; there is a large amount of literature associated with MOFs that experience significant structural deformation upon adsorption, heating, or other external stimuli.[15−17] In materials where framework flexibility is expected to be large, it would be necessary to perform calculations using our methods for a range of possible crystal structures before firm conclusions on the factors controlling molecular diffusion could be reached. In the many materials where framework flexibility is small, however, deviations from the experimental crystal structure due to adsorption could still play an important role in the motion of molecules that experience large energy barriers to diffusion. DFT calculations can play a useful role here, since the repulsive interactions that control the energy of a molecule moving through a transition state in this situation are captured accurately with DFT.[9] This is one example of how detailed modeling methods can improve upon the precision of our initial screening once the potential value of a material has been demonstrated in the initial screening. A related issue is that our calculations are typically based on crystal-

(52) Xomeritakis, G.; Gouzinis, A.; Nair, S.; Okubo, T.; He, M.; Overney, R. M.; Tsapatsis, M. *Chem. Eng. Sci.* **1999**, *54*, 3521.
(53) Bonilla, G.; Tsapatsis, M.; Vlachos, D. G.; Xomeritakis, G. *J. Membr. Sci.* **2001**, *182*, 103.
(54) Vankelecom, I. F. J.; Dotremont, C.; Morobe, M.; Uytterhoeven, J. B.; Vandecasteele, C. *J. Phys. Chem. B* **1997**, *101*, 2154.
(55) Kim, S.; Pechar, T. W.; Marand, E. *Desalination* **2006**, *192*, 330.
(56) Hao, S.; Sholl, D. S. *Energy Environ.* **2008**, *1*, 175.

lographic data from which solvent molecules have been removed. This is only appropriate for materials that remain stable after solvent removal. Detailed consideration of a material must include studies of the activation procedures used to remove solvent and characterize the chemical state of any open metal sites or other reactive sites. In our view, this task is best approached experimentally. The same approach is necessary to establish the stability of materials relative to environmental factors (e.g., water). Again, the value of our screening approach is that it can provide a motivation to perform detailed studies of this kind.

Our geometrical methods are currently limited to examining spherical molecules. Extending our methods to rigid nonspherical molecules (e.g., CO_2) is certainly possible, but moving beyond this to flexible molecules is more challenging. Approaches suitable for examining larger molecules have been suggested[57,58] but are far more computationally demanding than the methods we have introduced. Despite this limitation, understanding the connection between the pore sizes of individual materials and the widely accepted kinetic diameters for small molecules that is provided by our results makes it possible to make useful qualitative predictions about a large range of nonspherical species without performing detailed calculations. Even for molecules with a significant degree of internal flexibility, it seems likely that many MOFs can be eliminated from any further analysis by comparing the calculated pore-limiting diameter based on spherical probes with the smallest dimension of the molecule in question. Categorizing a large number of MOFs in this sense would be useful for selecting a small number of materials for which detailed analysis using methods suitable for fully flexible molecules would be productive.

Our calculations of the Henry's constants for adsorption and the diffusion activation energy are only applicable to nonpolar adsorbates, since for these species a plausible set of nonbonded interatomic potentials can be defined (via the UFF) than can be used for all MOFs. To extend this approach to polar adsorbates, it would be vital to include a description of the Coulombic interactions between adsorbed molecules and the MOF. This poses a challenge because current approaches to assigning charges to atoms in MOFs for use in forcefield calculations require time-consuming quantum mechanical calculations for each MOF of interest.[23] Our results suggest that a useful way to approach this problem may be to screen a large number of MOFs for target applications involving polar adsorbates based on geometrical considerations alone, then use the results of this effort to focus attention on a handful of promising materials for which quantum chemistry calculations would then be performed.

Our calculations for adsorption and membrane selectivity for spherical adsorbates are based on a simplified description that is relevant in the Henry's law regime. The Henry's constant for an adsorbate gives a simple estimate of the range of partial pressures over which Henry's law is applicable. In this regime, only the self-diffusion coefficient is needed to fully describe molecular diffusion. To describe practical situations where higher pressures are important, well developed molecular simulation methods based on Grand Canonical Monte Carlo (for adsorption), and molecular dynamics and/or transition-state theory (for diffusion, including self-diffusion or collective diffusion leading to net mass transfer) are available.[24,26,30] These methods require significantly larger computational resources that the calculations we have reported here, but they will play a key role in completing a detailed evaluation of materials that are suggested to be of special interest. In the Henry's regime, mixture effects among adsorbates can (by definition) be neglected. Our geometric analysis already provides useful guidelines for avoiding situations where mixture effects could have severely negative consequences. In particular, it is desirable to consider materials in which the largest cavity diameter is significantly larger than the pore-limiting diameter. When this is the case, coadsorbed molecules should typically be readily able to pass one another in the pores, even when the overall diffusion of one or more species is very slow. Beyond this qualitative description, the molecular simulation methods just mentioned above can provide detailed information on the role of mixture effects at nondilute pore loadings.

Finally, we reiterate that comparing the predictions of our calculations for defect-free MOF crystals with experimental measurements of real materials can be nontrivial. One important avenue for applying MOFs for kinetic separations is to grow dense thin films for use as membranes. Just as in the literature on zeolite membranes, crystal orientation and microstructure may ultimately play a critical role in the performance of these devices. Our results for the intrinsic properties of MOF crystals should be valuable in this area by focusing attention on materials with significant promise for targeted applications and, ultimately, contributing to efforts to understand and control the influence of nonintrinsic properties in membranes.[39−44] Other avenues for exploiting MOFs in kinetic separations also exist, including using MOFs as components in polymer/MOF composite membranes and in cyclic operation of packed beds using processes designed to take advantage of adsorption kinetics.

Acknowledgment. This work was supported by ConocoPhillips Company.

Supporting Information Available: Table summarizing the most important results for a sample of 25 MOFs examined and figures illustrating several representative MOFs. This material is available free of charge via the Internet at http://pubs.acs.org.

JA1023699

(57) Gounaris, C. E.; Wei, J.; Floudas, C. A.; Ranjan, R.; Tsapatsis, M. *AIChE J.* **2010**, *56*, 61.
(58) Haranczyk, M.; Sethian, J. A. *Proc. Natl. Acad. Sci. U.S.A.* **2009**, *106*, 21472.